Flow boiling in straight heated tubes under microgravity conditions

Marine Narcy, Erik de Malmazet, Catherine Colin

ECI 8th International Conference on Boiling and Condensation Heat Transfer
Ecole Polytechnique Fédérale de Lausanne, 3-7 June 2012
Lausanne, Switzerland

FLOW BOILING IN STRAIGHT HEATED TUBES UNDER MICROGRAVITY CONDITIONS

Marine NARCY, Erik DE MALMAZET, Catherine COLIN*
*Author for correspondence
Institut de Mécanique des Fluides de Toulouse, Allée du Professeur Camille Soula
University of Toulouse
Toulouse, 31400, FRANCE
E-mail: colin@imft.fr

ABSTRACT

Forced convective boiling experiments of *HFE-7000* were conducted in earth gravity and under microgravity conditions. The experiment mainly consists in the study of a two-phase flow through a 6 mm diameter sapphire tube uniformly heated by an *ITO* coating. The parameters of the hydraulic system are set by the conditioning system and measurements of pressure drops, void fraction and wall temperatures are provided. High-speed movies of the flow are also taken. The data were collected in normal gravity and during a series of parabolic trajectories flown in an airplane. Flow visualizations, temperature and pressure measurements are analysed to obtain flow pattern, heat transfer and wall friction data.

Key Words: two-phase flow, microgravity, heat transfer, wall friction

INTRODUCTION

Background

Two-phase thermal systems are broadly used in various industrial applications and engineering fields: flow boiling heat transfer is common in power plants (energy production or conversion…), transport of cryogenic liquids and other chemical or petrochemical processes. Thus, the understanding of boiling mechanisms is of importance for accidental off-design situations. These systems take advantage of latent heat transportation, which generally enables a good efficiency in heat exchanges.

For that reason, two-phase thermal management systems are considered as extremely beneficial for space applications. Indeed, in satellites or space-platforms, the major thermal problem is currently to remove the vast heat amount generated by devices from the inside into the space, in order to ensure suitable environmental and working conditions. Moreover, the growing interest for space applications such as communication satellites and the increasing power requirements of on-board devices lead to an urgent need of sophisticated management systems capable to deal with larger heat loads. Since the heat transfer capacity associated with phase change is typically large and with a relatively little increase in temperature, this solution could mean decreased size and weight of thermal systems.

But boiling is a complex phenomenon which combines heat and mass transfers, hydrodynamics and interfacial phenomena. Furthermore, gravity consequently affects the fluid dynamics and may lead to unpredictable performances of thermal management systems. It is thus necessary to perform experiments directly in (near) weightless environments. Besides the ISS, microgravity conditions can be simulated by means of a drop-tower, a parabolic flight in aircraft or a sounding-rocket.

Literature review

Although flow boiling is of great interest for space applications under microgravity conditions, few experiments have been conducted in low gravity. These experiments provided a partial understanding of the boiling phenomena and have been mostly performed for engineering purposes such as the evaluation of ISS's hardware or two-phase loop stability. Moreover, flow boiling heat transfer experiments in microgravity (referred to as μ-g) require large heat loads and available space. They are subject to severe restriction in the test apparatus, do not last long and offer few opportunities to repeat measurements for repeatability, which could explain the lack of data and of coherence between existing measurements. Nevertheless, several two-phase flow (gas-liquid flow and boiling flow) experiments have been conducted in the past forty years and enabled to gather data about flow patterns, pressure drops, and heat transfers including critical heat flux and void fraction in thermohydraulic systems. Previous state of the art and data can be found in the papers of Colin et al. (1996), McQuillen et al. (1998), Ohta (2003), and Celata and Zummo (2009).

Several studies have been carried out under microgravity conditions in order to classify adiabatic two-phase flows by various patterns through observation and visualizations of the flow. Various patterns have been identified at different superficial velocities of liquid j_l and gas j_v, patterns which are also encountered in boiling flows: bubbly flow, slug flow and annular flow.

Transitions flows have been studied too: transition between bubbly and slug flow, and transition between slug and annular flow or frothy slug-annular flow. The determination of these transitions is of importance because the wall friction and wall heat transfer are very sensitive to the flow pattern. Colin et al. (1991) and Dukler et al. (1988) drew a map based on void fraction transition criteria to predict patterns in liquid-gas flows. These patterns were also observed in boiling convective for heat transfer smaller than the critical heat flux by Ohta (2003), Lebaigue et al. (1998), Reinarts (1993) and more recently by Celata and Zummo (2009). The transition between bubbly and slug flows occurs from coalescence mechanisms. Coalescence can be promoted or inhibited depending of the value of the Ohnesorge number. A general flow pattern map for bubbly and slug flows based on the value of the Oh number was proposed by Colin et al (1996) for air-water flow and also boiling refrigerants. The transition between slug and annular flow has also been investigated by several authors, who proposed criteria based on transition void fraction value (Dukler at al., 1988), critical value of a vapour Weber number (Zhao and Rezkallah, 1993), balance between gas inertia and surface tension (Reinarts, 1993; Zhao and Hu, 2000).

The estimation of void-fraction or averaged gas velocity is a key-point for the calculation of wall and interfacial frictions. Different methods have been used to determine the cross-sectional averaged void fraction α: capacitance probes (Elkow and Rezkallah, 1997), conductance probes (Colin et al., 1991; Colin and Fabre, 1995; Bousman and Dukler, 1994) or flow visualisations (Lebaigue et al., 1998). It has been shown that the mean gas velocity $U_v = j_v/\alpha$ is well predicted by a drift flux model $U_G = C_0 . j$ for bubbly and slug flow (Colin et al., 1991), j being the mixture velocity and C_0 a coefficient depending on the local void fraction and gas velocity distributions.

Concerning the measurements of the wall shear stress, most of the studies performed under microgravity conditions concern gas-liquid flow without phase change (Bousman and McQuillen, 1994; Zhao and Rezkallah, 1995; Colin et al., 1996). Some results also exist for liquid-vapour flow (Chen et al., 1991), but in an adiabatic test section. The frictional pressure drop has been compared (Zhao & Rezkallah, 1995; Chen et al., 1991) to different empirical models (homogeneous model, Lockhart and Martinelli (1949)). Recently, Awad and Musychka (2010) proposed a modified correlation of Lockhart and Martinelli and found a good agreement with the experimental data. Very few studies reported data on the interfacial shear stress in annular flow (Dukler et al., 1988). This can be explained by the fact that such a measurement is based on pressure drop and liquid film thickness measurements which remains a difficult task.

Few researches on flow boiling heat transfer have been conducted, mainly because of the restrictive experimental conditions. Lui et al. (1994) carried out heat transfer experiments in subcooled flow boiling with *R113* through a tubular tests section (12 mm internal diameter, 914.4 mm length). Heat transfer coefficients were approximately 5 to 20 % higher in microgravity, generally increasing with higher qualities, which was believed to be caused by the greater movement of vapour bubbles on the heater surface. Ohta et al. (1995, 1997, and 2003) studied flow boiling of *FC-72* and *R113* in vertical transparent tubes (4,6 and 8 mm internal diameters), internally coated with a gold film, both on ground and during parabolic flight campaigns, and for a future experiment in the ISS. Authors examined various patterns and the influence of gravity levels on heat transfer coefficients for two-phase forced-convection heat transfer regime. It was noticed that the influence of gravity is not evident for high mass fluxes (G superior to 250 $kg.s^{-1}.m^{-2}$). This observation was also made by Baltis, Celata and Zummo (2009) who performed subcooled flow boiling experiments with *FC-72* in Pyrex tubes (2, 4 and 6 mm internal diameters). It was shown that the heat transfer coefficient decreases by up to 30-40% in microgravity in comparison with terrestrial gravity and that an increase of mass or heat flux seems to reduce the influence of gravity. A new technique for the measurement of heat transfer distributions has also been developed: Kim and al. (2012) used an IR camera to determine the temperature distribution within a multilayer consisting of a silicon substrate coated with a thin insulator. Work has still to be done to confirm and give coherence to the previous results of the literature on flow boiling and to compare the data sets obtained by the different authors.

Objectives

In this work, the authors intend to collect, analyse and compare flow boiling data in normal gravity or under microgravity conditions, thanks to a parabolic flight campaign. The working fluid is the *HFE-7000* which circulates in a heated test section made up of a 6 mm inner diameter sapphire tube with a conductive transparent *ITO* coating. Flow patterns, void fraction, film thickness, wall friction and heat transfer are studied.

This paper presents the preliminary results of the measurement campaigns within three major sections. The first section describes the experimental apparatus and the measurement techniques and accuracy. The data reduction to obtain the mass quality, gas velocity, heat transfer coefficient and wall shear stress is described in a second section. Finally the experimental results obtained in μ-g and 1-g experiments are presented and discussed.

EXPERIMENTAL TEST SETUP

Experimental apparatus

The experimental set-up mainly consists of a hydraulic loop which is represented in Figure 1. In this pressurized circuit, the working fluid is the refrigerant 1-methoxyheptafluoropropane ($C_3F_7OCH_3$), which will be referred as *HFE-7000*. It is first pumped at liquid state by an Iwaki gear pump while the liquid flow rate is measured by a Micromotion Coriolis flowmeter. The fluid is heated to its boiling point and partially vaporized in two serial heaters. Then it enters a stainless steel tube of 6 mm diameter and 22 cm length just upstream the test section. In the test section, the *HFE-7000* is further vaporized in a 6 mm diameter sapphire tube heated through an outside *ITO* coating (ascending flow). The fluid is then condensed and cooled down 10°C below its boiling point into four cold plates including Peltier modules and fans before it enters the pump again. The pressure is adjusted in the circuit via a volume compensator, whose bellow can be pressurized by air.

The *HFE-7000* has been chosen as working fluid for safety reasons and because of its low saturation temperature at atmospheric pressure (34°C at 1 bar) and its low latent heat of vaporization. It is a dielectric and non-toxic refrigerant too. In the circuit, the *HFE-7000* may be in a liquid or a liquid-vapour state depending on the portion of the hydraulic circuit, but it is never in a pure vapour state. The loop pressure is set from 1 to 2 bars and the fluid circulates with mass fluxes G between 100 and 1000 $kg.s^{-1}.m^{-2}$. A wide range of flow boiling regimes is studied, from subcooled flow boiling to saturated flow boiling, by adjusting the power input of the heaters (maximal power 900 W, vapour mass qualities up to 0.9) and the power of the *ITO* coating. The wall heat flux ranges from 0 to 45 000 $W.m^{-2}$.

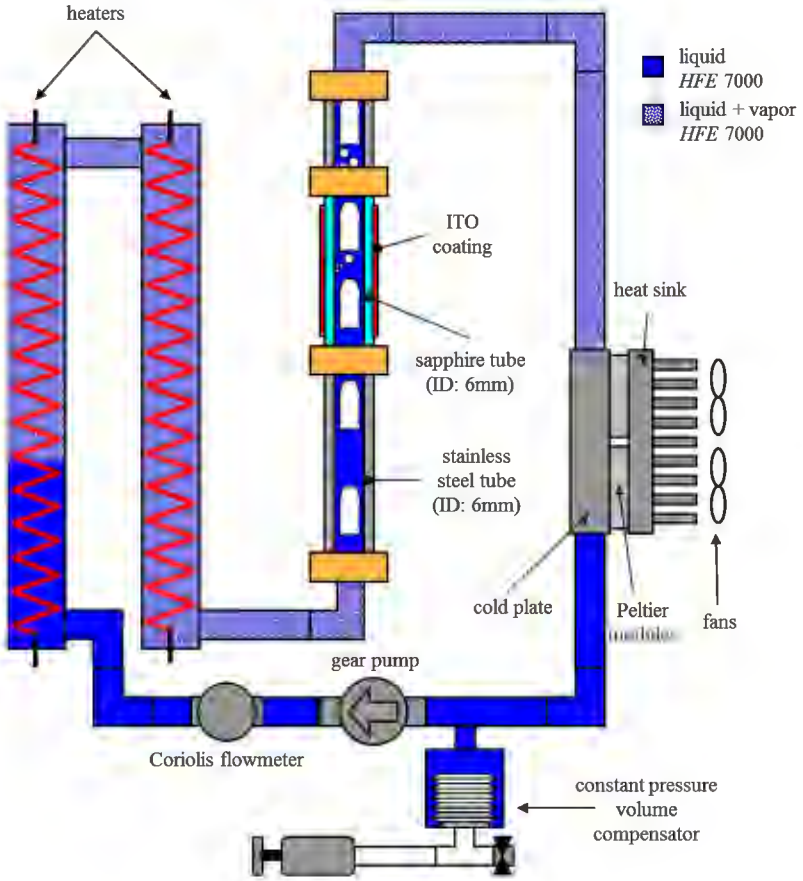

Figure 1 Schematic of the experimental apparatus.

The test section is represented in Figure 2. It mainly consists of a 20 cm long sapphire tube with an inner diameter of 6 mm and a thickness of 1 mm. The outer surface is almost totally coated with *ITO*, an electrical conductive and transparent coating which enables a uniformly heating by Joule effect and a visual display of the flow.

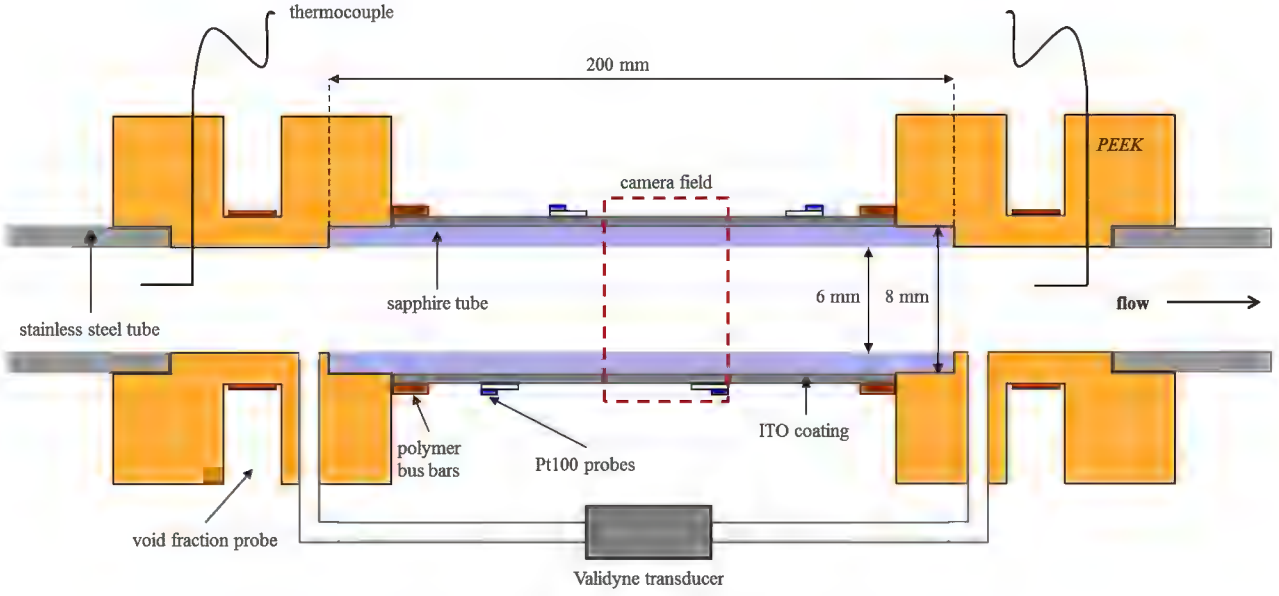

Figure 2 Schematic of the test section.

Measurement techniques

The conditioning system and the measurement system are composed of various measurement instruments such as temperature, pressure or void fraction sensors, a high speed camera, etc…

• Temperature - Two kinds of temperature sensors are used: thermocouples and Pt100 probes. The type K thermocouples are mainly used to measure the flow temperature at the heaters and test section inlet and outlet, with a precision of ± 0.2°C. They are calibrated with the Pt100 probes which measure the ambient temperature and the temperature of the external surface of the sapphire tube at four different positions, with a precision of ± 0.1°C.

• Pressure - Two absolute pressure sensors are located at the pump and test section inlets and are used to calculate the saturation temperature. Two differential pressure transducers Validyne P305D measure the pressure drop along the sapphire tube with a precision of ± 0.5 mbar; they are calibrated at *IMFT* using two manometers with different ranges.

• Void fraction – The void fraction is the volume fraction of the vapour phase. Two void fraction probes are inserted into the test section's inlet and outlet. One of them is represented in Figure 3 *(a)*. Void fraction sensors are composed of two copper electrodes of 1 cm² area used for a capacitive measurement and are developed at *IMFT*. The principle of these probes is to measure the capacitance between the electrodes which depends on the fraction of liquid and vapour in the tube section between the electrodes. The calibration is performed by using liquid *HFE-7000* and Teflon rods which have approximately the same permittivity as vapour *HFE-7000*. Rods of various diameters are used for the calibration. The Teflon rod is located in the middle of the pipe section, surrounded by liquid *HFE-7000* in order to mimic the annular flow configuration. Since the capacitance measurement is strongly dependant of the flow pattern, direct calibrations are also performed in bubbly flow by measuring the bubble velocities from image processing of the high speed-videos. The calibration curve is shown in Figure 3 *(b)*.

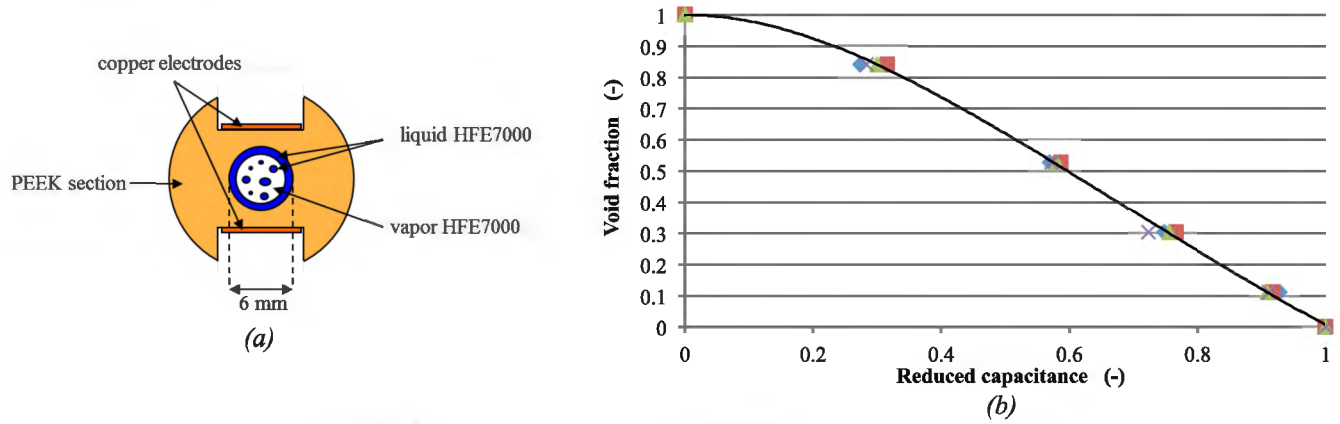

Figure 3 Void fraction probes *(a)* Schematic *(b)* Calibration curve.

• Flow visualization – A high speed video camera PCO 1200 HS with the associated backlight source is used to obtain movies of the flow through the transparent coating of the sapphire tube. The camera field of view is 1000*350 pixels² large and the acquisition frequency is 1000 or 1500 images per second. The spatial resolution of the images is 0.03 mm/pixel.

The acquisition system consists of a 36 channels National Instrument data acquisition system, two laptops with LabVIEW interfaces and a computer for the acquisition of the camera images using the Cameware software.

Measurement campaigns

Experiments were conducted both on ground and under microgravity conditions. A weightless situation is simulated during a parabolic flight campaign which consists of three flights with around 31 parabolas per flight. Each parabola provides up to 22 seconds of microgravity with a gravity level smaller than 3.10^{-2} g. Parabolic flight campaigns are the only sub-orbital opportunity for experimenters to work directly on their experimental apparatus under microgravity conditions and without being too limited by the size of their set- up and the available power on board.

During the on-ground measurement campaign, relevant parabolas were reproduced in order to compare data obtained in normal gravity and under microgravity conditions. A series of parametric runs has also been conducted to complete the database.

DATA REDUCTION

Balance equations

Hereafter, the calculations of heat transfer coefficients, vapour quality and wall friction are presented. These values are deduced from the measurements of wall and liquid temperatures, heat flux, pressure drop and void fraction by using mass, momentum and enthalpy balance equations.

> Calculation of the heat transfer coefficient

A cross-section of the sapphire tube is represented in Figure 4. T_{iw} and T_{ow} are the inner and outer temperatures of the sapphire tube wall, respectively. $T_{e\infty}$ is the external temperature far from the tube ("at infinity") and $T_{i\infty}$ is the fluid bulk temperature in the tube far from the wall. T_{in} and T_{out} are the liquid bulk temperatures at the inlet and outlet of the sapphire tube.

The inner and outer radii of the sapphire tube are denoted by R_i and R_o, respectively. The sapphire thermal conductivity is denoted by k.

The *ITO* coating on the external surface of the test section provides a heat flux q_{ow}. The heat flux q_{iw} delivered to the fluid is considered as equal to q_{ow} corrected by the radii ratio R_o/R_i. The heat transfer between the internal flow and the internal wall of the sapphire tube is characterized by the heat transfer coefficient h_i. The heat transfer between the environment and the external wall of the sapphire tube (thermal losses) is characterized by the heat transfer coefficient h_e.

Following hypotheses are made: 1) Temperature profiles are axisymmetric. 2) The axial conduction can be neglected. 3) The heat transfer by radiation can be neglected.

An energy balance in steady state between the inner and outer walls of the sapphire tube leads to expressions (E1) and (E2).

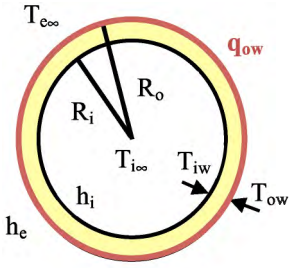

Figure 4 Notations.

$$T_{ow} - T_{iw} = [q_w - h_e.(T_{ow} - T_{e\infty})].\frac{\ln\left(\frac{R_o}{R_i}\right).R_o}{k} \quad (E1)$$

$$h_i.(T_{iw} - T_{i\infty}) = \frac{R_o}{R_i}.[q_{ow} - h_e.(T_{ow} - T_{e\infty})] \quad (E2)$$

The temperature evolution between T_{in} and T_{out} is considered as linear, which enables to calculate $T_{i\infty}$.

A series of experiments has been conducted in order to evaluate the thermal losses through the coefficient h_e. In particular, h_e can be locally estimated in normal gravity with the local measurement of T_{ow} and the measurement of $T_{e\infty}$ for single or two-phase flow without heating by using a known correlation to estimate h_i.

$$h_e = \frac{T_{i\infty} - T_{ow}}{\left(\frac{\ln\left(\frac{R_o}{R_i}\right).R_o}{k} + \frac{1}{h_i}.\frac{R_o}{R_i}\right)(T_{ow} - T_{e\infty})} \quad (E3)$$

In this configuration, thermal losses have been estimated for single and two-phase flows with different correlations. The maximal heat transfer coefficient h_e that was obtained in normal gravity represents 7% of heat transfer coefficient h_i. Future experiments with single-phase flows characterized by very low mass fluxes G and high temperatures should allow to conclude about the nature of thermal losses, through a global energy balance.

If thermal losses are neglected, the heat transfer coefficient h_i can be expressed in function of q_{iw}, T_{ow} and $T_{i\infty}$.

> Calculation of vapour quality

The vapour quality can be calculated by using the total enthalpy conservation equation in steady state. q_{iw} is the wall heat flux delivered to the fluid by Joule effect through the *ITO* coating, and D_i is the inner diameter of the sapphire tube.

• for saturated boiling regimes: if T_l is the liquid temperature, $T_l = T_{sat}$, which leads to the expression (E4). The evolution of the mass quality can be directly calculated with the wall heat flux and the vapour quality at the inlet of the test section is considered as equal to the vapour quality at the outlet of the heaters.

$$\frac{4.q_{iw}}{D_i} = G.\Delta h_{l,v}.\frac{dx}{dz} \quad (E4)$$

Considering that the wall heat flux is constant, a linear evolution of vapour quality is observed. The vapour quality at the inlet of the test section is deduced from an energy balance in the preheaters. In this case, the vapour quality calculated with the total enthalpy conservation equation is equal to the classical thermodynamic vapour quality.

• for subcooled boiling regimes, we have $T_l < T_{sat}$ and the vapour temperature is assumed to be equal to the saturation temperature. The enthalpy balance equation for the mixture can be written:

$$\frac{4.q_{iw}}{D_i} = \frac{d}{dz}\left(\rho_v.\alpha.U_v.h_{v,sat} + \rho_l.(1-\alpha).U_L.h_L\right) = \frac{d}{dz}\left(G.[x.h_{v,sat} + (1-x).\left(h_{l,sat} + Cp_l.(T_l - T_{sat})\right)]\right) \quad (E5)$$

where h_l is the liquid enthalpy and $h_{v,sat}$ and $h_{l,sat}$ are the vapour and liquid enthalpies at saturation temperature, respectively.

The wall heat flux leads to an increase of the total enthalpy of the mixture, both by phase change and by increasing the liquid temperature:

$$\frac{4.q_{iw}}{D_i} = G.\left(\Delta h_{l,v} + Cp_l.(T_{sat} - T_l)\right).\frac{\partial x}{\partial z} + G.Cp_l.(1-x).\frac{\partial T_l}{\partial z} \quad (E6)$$

For the experiments in subcooled boiling, a single-phase flow is observed at the inlet of the test section. Indeed, a 22 cm long stainless steel tube enables to condensate potential bubbles coming from the two serial heaters. Then the inlet quality is 0 and equation (E6) can be integrated as followed:

$$x(z) = \left(1 - \frac{4.q_{iw}.D_e}{G.D_i^2.Cp_l.\frac{T_{out} - T_{in}}{L_{heated}}}\right).\left(1 - e^{\frac{Cp_l.(T_{out} - T_{in})}{h'_{l,v}.L_{heated}}.z}\right) \quad (E7)$$

where $h'_{l,v} = \Delta h_{l,v} + Cp_l.(T_{sat} - T_l)$ (E8)

For both cases, the fluid temperature is measured at the inlet and outlet of the test section and the temperature evolution between these two points is considered as linear.

The calculation of the vapour quality in subcooled boiling is tricky because of the order of magnitude of x and of measurement uncertainties. We can define measurement errors Δq_w on the measured wall heat flux and ΔT_l on the measured liquid temperature. Measurement errors on mass flux G, and geometrical and physical properties are neglected. By considering the equation (E6), the error Δx on a low vapour quality can be expressed:

$$\Delta x \approx \frac{4.\Delta q_w}{D_i}.\frac{L_{heated}}{G.\Delta h_{l,v}} + \frac{Cp_l}{\Delta h_{l,v}}.\Delta T_l \qquad \text{(E9)}$$

$$\Delta x = 4.\frac{10^3}{6.10^{-3}}.\frac{16.10^{-2}}{8.10^2.14.10^4} + \frac{13.10^2}{14.10^4}.2.10^{-1}$$

$$\Delta x \propto 2.10^{-3}$$

The error on the vapour quality is 2.10^{-3}, which is the order of magnitude of x itself. This error was confirmed by an analysis of flow videos using void fraction and superficial velocities considerations.

> Calculation of the wall friction

The two differential pressure transducers Validyne P305D measure the pressure drop ΔP along the test section (heated section with the sapphire tube plus adiabatic lengths in the thermoplastic at the inlet and outlet of the tube). The momentum balance equation in steady state enables to write the wall friction according to the pressure drop, the void fraction, the mass flux and the vapour quality:

$$\frac{dP}{dz} = \underbrace{\frac{4}{D}.\tau_p}_{\text{friction}} - \underbrace{\frac{d}{dz}\left[\frac{G^2.x^2}{\rho_V.\alpha} + \frac{G^2.(1-x)^2}{\rho_L.(1-\alpha)}\right]}_{\text{acceleration}} - \underbrace{g.[\rho_V.\alpha + \rho_L.(1-\alpha)]}_{\text{gravity}} \qquad \text{(E10)}$$

(τ_p negative)

The acceleration term only appears in the heated section of the test section. By integrating the equation (E10) between the inlet and the outlet of the test section, the wall friction can be expressed according to the pressure difference measured by the differential Validyne, the mass flux, the vapour quality and the void fraction:

$$\Delta P = -\frac{4}{D}.\int_{inlet}^{outlet} \tau_w.dz + G^2.\left[\frac{x^2}{\rho_V.\alpha} + \frac{(1-x)^2}{\rho_L.(1-\alpha)}\right]_{heated\ inlet}^{heated\ outlet}$$

$$+ g.\int_{inlet}^{outlet} (\rho_V.\alpha(z) + \rho_L.(1-\alpha(z))).dz \qquad \text{(E11)}$$

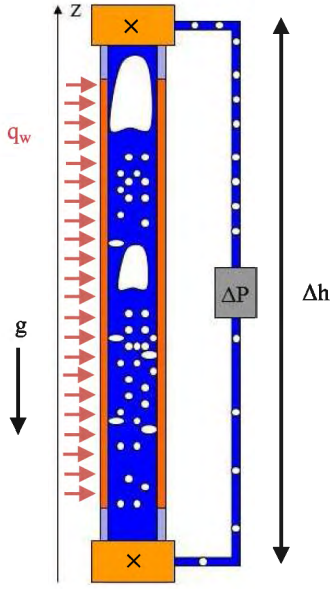

Figure 5 Pressure drop measurement.

The wall friction can only be determined along the whole test section (heated and adiabatic sections). ΔP is measured by the differential Validyne transducers (there is no vapour in transmissions lines); x is calculated at the inlet and outlet of the sapphire tube with energy balances and α is measured at the inlet and outlet of the test section by two void fraction probes.

In μ-g, the last term of equation (E11) can be neglected. On ground, in vertical flow, the last term is dominant, thus the accuracy on the wall shear stress measurement is directly linked to the accuracy on the void fraction measurement itself.

Validations for single-phase flow

Measurements for single-phase flows in normal gravity have enabled to validate the measurement technics and calculation protocols by confronting the data to standard correlations.

> Pressure drops

For the wall friction coefficient f_w in single-phase flow in normal gravity, the Blasius correlation based on the global Reynolds number Re is used:

$$f_w = 0{,}0791.Re^{-0{,}25} \qquad \text{(E12)}$$

The Figure 6 shows the measurements obtained with the two differential Validyne transducers in 1-g for single-phase flows with various mass fluxes and the Blasius' correlation with error bars at +10 % and –10%.

For a sample of fifteen measurements points, the experimental data meet the Blasius' correlation with a maximal error of 13% and an averaged error of 8%, for the two sensors, which is a satisfying precision.

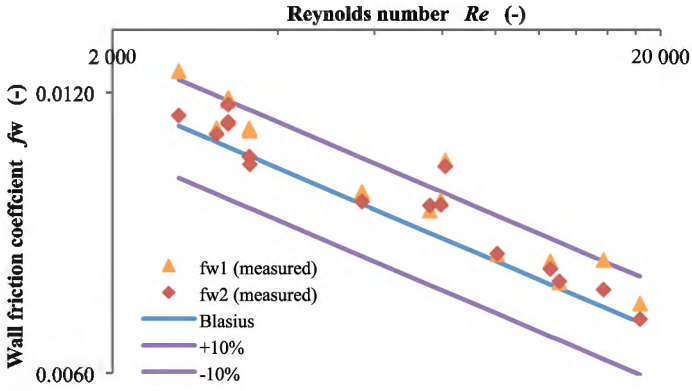

Figure 6 Wall friction coefficient in single-phase flow (measurements and Blasius' correlation).

> Heat transfer coefficient

For the fully developed turbulent flow Nüsselt number Nu_∞ in single-phase flow in normal gravity, the Dittus and Boelter's correlation and the Gnielinski's correlation based on the global Reynolds number Re and Prandtl number Pr are used. The wall friction coefficient f_w is calculated with the Blasius' correlation. z is the distance between the probe and the inlet of the heated section and D_h is the hydraulic diameter which is equal to the inner diameter D_i.

Investigators	Correlations	Application range
Dittus and Boelter	$Nu_\infty = 0.024.Re^{0.8}.Pr^{0.4}$	Fully developed turbulent flow, $L/d > 60$ $0.7 \le Pr \le 120$ and $2500 \le Re \le 1.24.10^5$
Gnielinski	$Nu_\infty = \frac{(f_w/2).(Re-1000).Pr}{1+12{,}7.(f_w/2)^{1/2}.(Pr^{2/3}-1)}$	Fully developed turbulent flow $0.5 \le Pr \le 2000$ and $2300 \le Re \le 5.10^6$
Al-Arabi	$\frac{Nu_m}{Nu_\infty} = 1 + \frac{C}{z/D_h}$ $C = \frac{(z/D_h)^{0,1}}{Pr^{1/6}}\left(0{,}68 + \frac{3000}{Re^{0,81}}\right)$	Thermally developing flow $Pr > 0{,}2$

Table 1 Nüsselt correlations for fully developed and thermally developing flows in smooth and circular ducts.

Figure 7 shows Nüsselt numbers corresponding to the four Pt100 probes located on the outer surface of the sapphire tube for various mass fluxes in single-phase flows. The Gnielinski's correlation and two error bars at +15% and -15% are also plotted. The deviation from the correlation is in inverse proportion to the distance between the temperature sensors (1, 2, 3 or 4) and the inlet of the heated section; hence the hypothesis of a thermally developed flow in the sapphire tube is not satisfied.

Whenever the flow is thermally developing, a local heat transfer coefficient corresponding to a mean Nüsselt number Nu_m is measured. This number must be corrected according to the distance between the measurement point and the inlet of the heated section in order to calculate the fully developed flow Nüsselt number Nu_∞ and to compare it with correlations. Figure 8 shows the measurements corrected with Al-Arabi's correlation and compared to the Gnielinski's formula (Table 1).

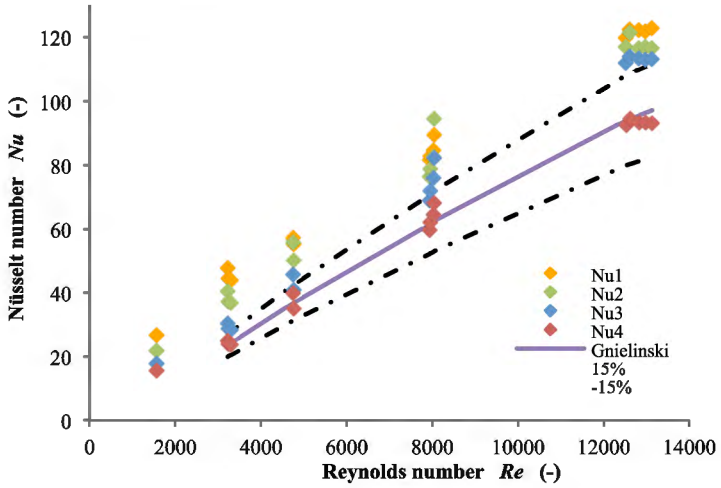

Figure 7 Measured Nüsselt number and Gnielinski's correlation for fully developed single-phase flows.

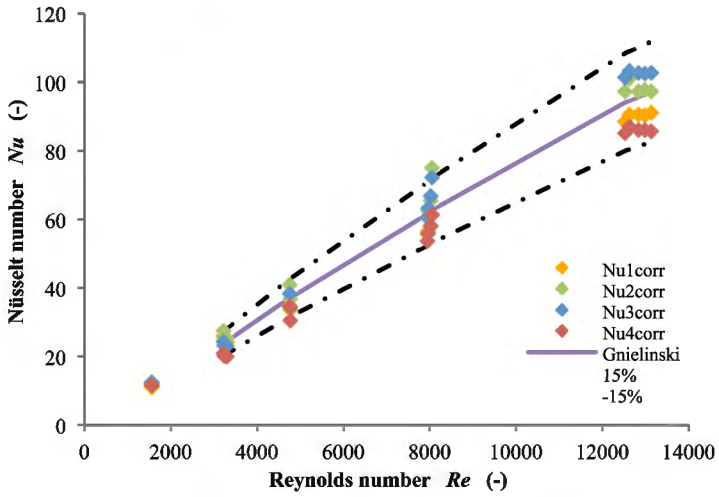

Figure 8 Measured Nüsselt number and Gnielinski's correlation with Al-Arabi's correction.

The experimental data corrected according to the sensor position meet the Gnielinski's correlation with a maximal error of ±17%. The error depends of the mass flux (that varies the thermal entrance length) and of the probe position. The precision between measurements and correlations is satisfying for the whole set of experiments in single-phase flow. It also confirms the weak impact of external thermal heat losses on the measurements.

RESULTS AND DISCUSSION

Preliminary results about flow patterns, heat transfer coefficients and wall friction are presented. Data about void fraction and film thickness are currently under reduction.

Flow patterns

The high speed camera has enabled to visualize flow patterns for various mass fluxes G, vapour qualities x at the inlet of the test section and heat fluxes q_{ow} through the *ITO* coating. Similar flow patterns have been observed in normal gravity and microgravity: annular flow, slug flow and bubby flow were distinguished in videos.

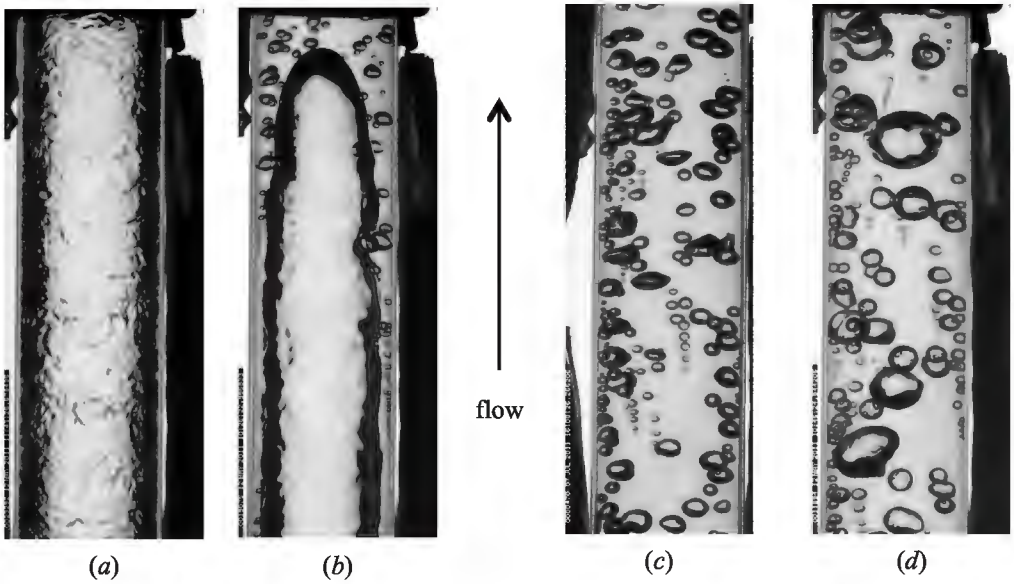

Fig 9 Flow visualizations.

(*a*) annular flow in μ-g
(*b*) slug flow in μ-g

(*c*) bubbly flow in 1-g
(*d*) bubbly flow in μ-g
G = 280 kg.s^{-1}.m^{-2},
p = 1.2 bar, ΔT_{sub} = 13 K,
q_{ow} = 19 600 W.m^{-2}

Figure 9 shows annular flow and slug flow with nucleated boiling in μ-g and a comparison between bubbly flows in 1-g and μ-g for the same parameters (G, x and q_{ow}). Bubbly flows correspond to subcooled regimes ($T_l < T_{sat}$). The impact of gravity level on the bubbles size and shape can be seen in the videos for mass fluxes inferior to 400 kg.s^{-1}.m^{-2}: under microgravity conditions, bubbles are larger than in normal gravity and are not deformed by the gravity field. The larger bubble size in microgravity can be explained by both the larger bubble diameter at detachment and the higher rate of coalescence. A vapour quality increase leads through a coalescence phenomenon to slug flow which alternates between long Taylor bubbles and liquid plugs that can be aerated by small bubbles. Coalescence of long Taylor bubbles indicates the transition to annular flows which always correspond to saturated regimes (T_l=T_{sat}). The precision of the flow parameters setting and the camera spatial resolution do not enable to see clearly differences between 1-g and μ-g in the videos for annular flows.

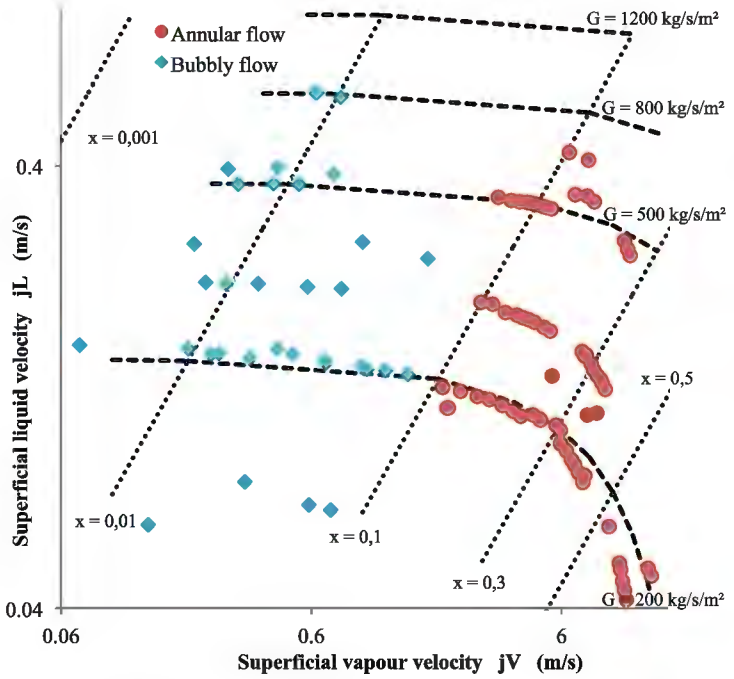

Figure 10 Flow pattern map for the experiments in 1-g

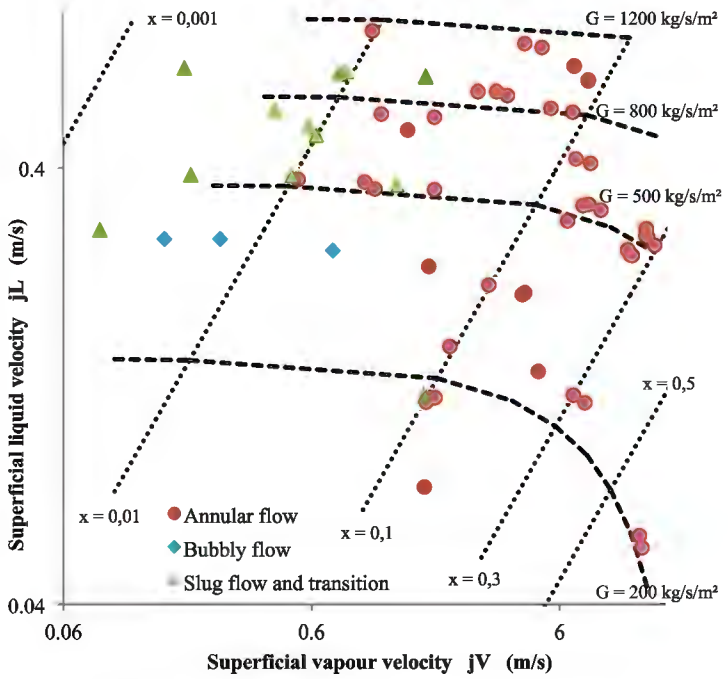

Figure 11 Flow pattern map for the experiments in μ-g

Figures 10 and 11 show flow patterns maps for the experiments performed in normal gravity and under microgravity conditions, respectively. Regimes are indicated according to the superficial vapour and liquid velocities, and iso-curves for G and x are added. Because of the uncertainty about the calculation of the vapour quality, experimental points for x inferior to 0.001 are not shown. Figure 11 presents relevant parabolas performed during the flight campaign for mass fluxes up to 1200 kg.s^{-1}.m^{-2}. A preliminary data reduction has underlined the fact that gravity effect was not clearly quantifiable for mass fluxes G superior to 400 kg.s^{-1}.m^{-2}. Therefore, no experiments and parametric runs were performed in 1-g for G > 800 kg.s^{-1}.m^{-2}.

In normal gravity, the transition between bubbly and annular flow occurs very fast for low mass fluxes, typically at x around 0.1. For higher mass flux, this transition seems to last within a larger x range but that was not further investigated. Bubbly and slug flows evolve toward annular flow earlier in microgravity than in normal gravity because of the more important coalescence phenomenon.

Wall friction

In microgravity, the gravity term of Equation (E6) can be neglected. Therefore, the wall friction can be directly deduced from the pressure drop measurement, after subtraction of the inertia term.

Preliminary reduction using Martinelli's relationship for the determination of α has shown that the inertia term represents up to 20% of the pressure drop and cannot be neglected in the global balance. The calculation of the wall friction term was conducted by taking this consideration into account.

Figure 12 represents the experimental two-phase frictional multiplier Φ_l^2 in microgravity compared to the one predicted by the Lockhart and Martinelli's correlation (1949). X is the Martinelli's parameter.

$$X = \frac{j_l}{j_v} \cdot \sqrt{\frac{\rho_l}{\rho_v} \cdot \frac{f_{wl}}{f_{wv}}} \qquad \text{(E13)}$$

$$\Phi_l^2 = \left(1 + \frac{20}{X} + \frac{1}{X^2}\right) \qquad \text{(E14)}$$

Experimental data meet the theoretical relationship but with a certain dispersion (standard deviation of 15.4%).

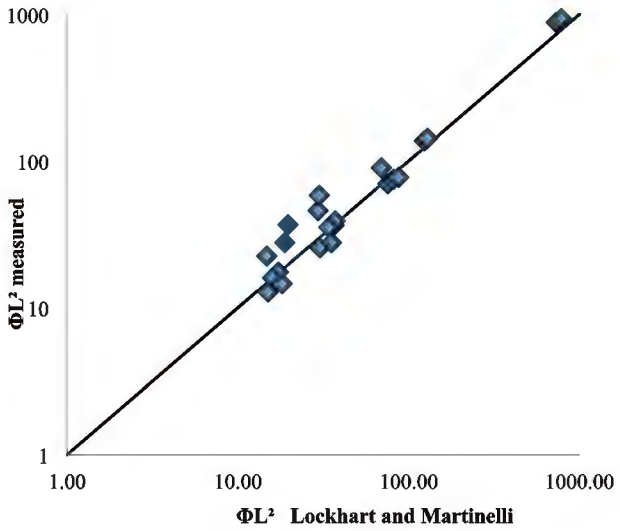

Figure 12 Comparison between experimetal and theoretical multipliers in μ-g from Lockhart and Martinelli correlation.

Heat transfer coefficients

Heat transfer coefficients in 1-g and in μ-g for saturated boiling regimes are presented in Figures 13 and 14.

The precision of the calculation of h_i is directly linked to the measurement accuracy of q_{ow} and of temperatures (wall and liquid bulk temperatures) and to the chosen evolution of the temperature in the sapphire tube between T_{in} and T_{out}. By using a linear evolution of the temperature in the heated section and by considering uncertainties Δq_w and ΔT on the heat flux and temperatures, respectively, heat transfer coefficients can be calculated with an error bar at ±8%.

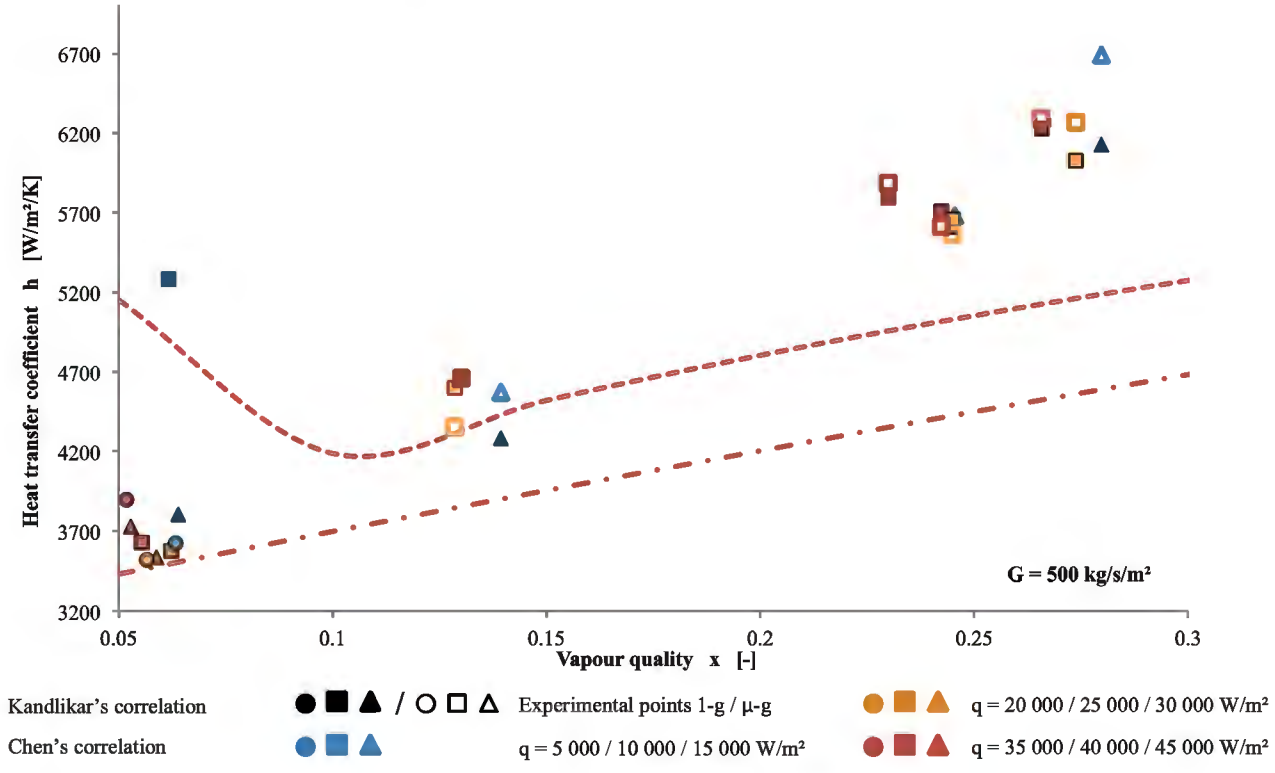

Figure 13 Heat transfer coefficients according to the vapour quality for G = 500 kg.s^{-1}.m^{-2} and for various heat fluxes in 1-g and μ-g compared to Kandlikar and Chen correlations at q_{ow} = 35 000 W/m².

Figure 13 shows heat transfer coefficients according to the vapour quality for G = 500 kg.s^{-1}.m^{-2} for saturated boiling regimes. h_i in subcooled boiling regimes are not presented because it was not possible to evaluate accurately the local quality at the different positions of the heated section. Colour and shape codes enable to distinguish various heat fluxes ranging from 5 000 W/m² to 45 000 W/m² and some experimental points in μ-g are indicated with their on-ground equivalents.

Measurements in normal gravity are compared with two boiling heat transfer relationships: Chen's correlation (1966) and Kandlikar's correlation (1989) which brings into play the boiling number, the Froude number and a coefficient linked to the Martinelli's parameter. At fixed mass flux, the evolution of h_i on ground is the expected one: the heat transfer coefficient increases with the vapour quality at fixed heat flux, and increases with heat flux at fixed vapour quality. At low vapour quality, experimental points meet the correlations, but for higher x, the heat transfer coefficients are higher than predicted in 1-g.

At G = 500 kg.s^{-1}.m^{-2}, the effect of gravity level on boiling heat transfer cannot be quantifiable given the measurement uncertainties: the mean difference on h_i between 1-g and μ-g for G = 500 kg.s^{-1}.m^{-2} is ±3.5%.

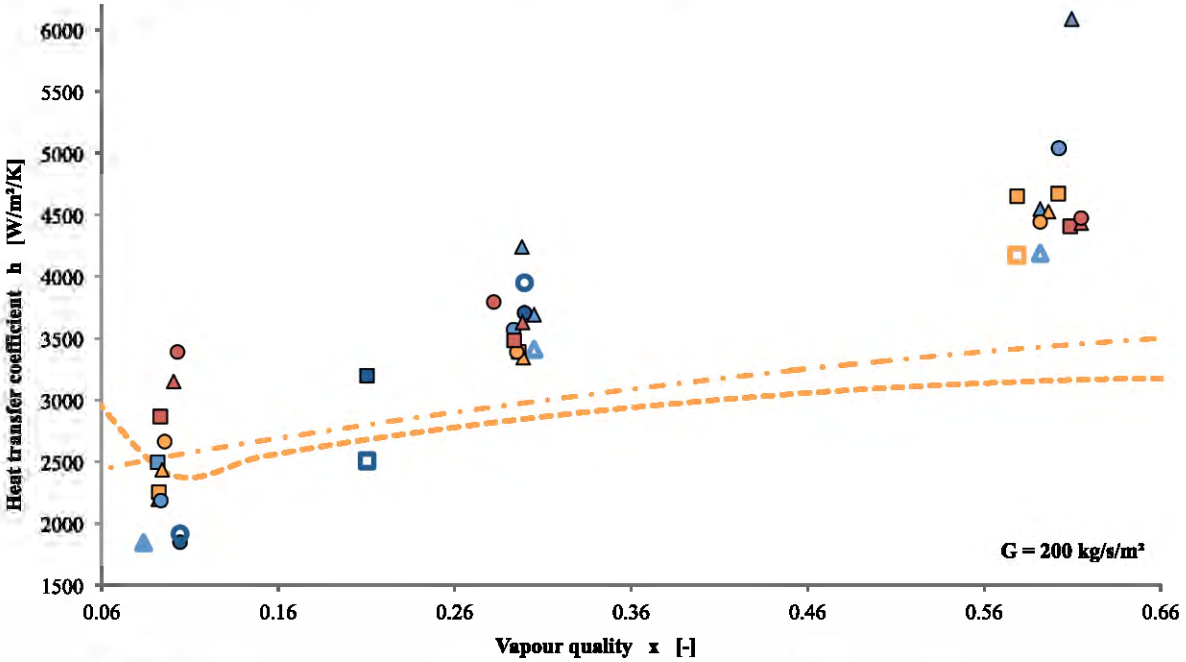

Figure 14 Heat transfer coefficients according to the vapour quality for G = 200 kg.s^{-1}.m^{-2} and for various heat fluxes in 1-g and μ-g compared to Kandlikar and Chen correlations at q_{ow} = 20 000 W/m².

Figure 14 shows heat transfer coefficients according to the vapour quality for G = 200 kg.s^{-1}.m^{-2} for saturated boiling regimes. The same colour and shape codes than the one in the Figure 13 enable to distinguish various heat fluxes ranging from 5 000 W/m² to 45 000 W/m² and some experimental points in μ-g are indicated with their on-ground equivalents.

Similar comments can be made about the evolution of heat transfer coefficient according to vapour quality or heat flux at fixed mass flux and about the comparison with correlations. Moreover, by comparing Figures 13 and 14, it can be shown that h_i also increases with mass flux at fixed vapour quality or fixed heat flux.

At G = 200 kg.s^{-1}.m^{-2}, the effect of gravity level on boiling heat transfer is more quantifiable than for higher mass rates: the mean difference on h_i between 1-g and μ-g for G = 200 kg.s^{-1}.m^{-2} is ±28% and the heat transfer coefficient tends to be smaller under microgravity conditions than in normal gravity. This trend has to be confirmed by additional experiments.

PERSPECTIVES AND CONCLUSIONS

This paper presents the results of flow boiling experiments performed under microgravity conditions during a parabolic flight campaign and compared to parametric runs conducted on ground. The objective was to collect heat transfer, void fraction and wall friction data along a heated test section consisting of a 6 mm inner diameter heated sapphire tube, using *HFE-7000* as working fluid.

Special attention was paid to the calculation of the vapour quality in order to characterize properly the subcooled boiling regimes, but the accuracy of this parameter is directly linked to the temperature measurement precision. For that reason, reduced flow patterns maps have been presented.

Annular flow, slug flow and bubbly flow have been observed in videos according to the vapour quality and the mass and heat fluxes. The transition between slug and annular flow seems to occur at lower qualities in microgravity. Significant differences in the heat transfer coefficient can be noticed according to the flow pattern. Heat transfer values are in good agreement with classical correlations of the literature at moderate qualities below 0.2, but are significantly higher for quality grater than 0.3. The results show that the gravity level has little impact on heat transfer for mass fluxes superior to 400 kg.s^{-1}.m^{-2} whatever the flow pattern is.

Flow boiling heat transfer rate at low mass fluxes under microgravity conditions can be either increased or reduced up to 30% but the lack of experimental points does not enable to conclude about gravity effect. Additional experiments at lower mass fluxes should be conducted in order to highlight a trend.

Another parabolic flight campaign will be the opportunity to perform new experiments in microgravity. Future test matrix plans to conduct runs at lower mass fluxes by adapting the hydraulic loop and to improve the accuracy on the temperature measurement for the calculation of the vapour quality and the reduction of void fraction data and flow visualizations.

ACKNOWLEDGMENT

The authors would like to acknowledge the French and European Space Agencies *CNES* and *ESA* for having funded this study and for their support in the parabolic flight campaigns.

NOMENCLATURE

Symbols

Cp	heat capacity, $J.K^{-1}.kg^{-1}$
D	tube diameter, m
g	gravitational acceleration, $m.s^{-2}$
G	mass flux, $kg.m^{-2}.s^{-1}$
h	heat transfer coefficient, $W.m^{-2}.K^{-1}$
$\Delta h_{l,v}$	enthalpy of vaporization, $J.kg^{-1}$
j	volumetric flux or superficial velocity, $m.s^{-1}$
Nu	Nusselt number, –
p	pressure, bar
q	heat flux, $W.m^{-2}$
R	radius, m
Re	Reynolds number, –
T	temperature, °C
x	vapour quality, –
ΔT	subcooling, °C

Greek Symbols

α	void fraction, –
ε	permittivity, –
ρ	density, m^3/kg^{-1}
τ	shear stress, Pa

Subscripts

e	environment
i	internal
in	inlet conditions
l	liquid phase
o	outer
out	outlet conditions
sat	saturation conditions
sub	subcooled conditions
v	vapour phase
w	wall

REFERENCES

Al-Arabi, M. (1982). Turbulent Heat Transfer in the Entrance Region of a Tube, *Heat Transfer Eng.*, (3): 76 – 83.

Awad M.M., Muzychka Y.S., (2010). Review and modeling of two-phase frictional pressure gradient at microgravity conditions, *Fluid Enginnering Division Summer Meeting ASME*, Montreal, August 2010.

Baltis, C.H.M., Celata, G.P., Zummo, G. (2009). Multiphase Flow Heat Transfer in Microgravity, *Internal communication.*

Blasius, H. (1913). Das Ähnlichkeitsgesetz bei Reibungsvorgängen in Flüssigkeiten, *Forschg. Arb. Ing.-Wes.*, (131): Berlin.

Celata, G.P., Zummo, G. (2009). Flow Boiling Heat Transfer in Microgravity: Recent Progress, *Multiphase Science and Technology*, Vol. 21, No. 3, pp. 187–212.

Chen, I.Y., Downing, R.S., Keshock, E., Al-Sharif, M. (1991). Measurements and correlation of two-phase pressure drop under microgravity conditions, *Journal of Thermophysics,* **5**, 514-523.

Colin, C., Fabre, J., Mc Quillen, J. (1996). Bubble and slug flow at microgravity conditions: state of knowledge and open questions, *Chem. Engng. Com.,* **141-142**, 155-173.

Colin C., Fabre, J. , Dukler, A.E. (1991). Gas-Liquid flow at microgravity conditions-I: Dispersed bubble and slug flow, *Int. J. Multiphase Flow,* 17, 533-544, 1991.

Colin, C., Fabre, J. (1995). Gas-liquid pipe flow under microgravity conditions: influence of tube diameter on flow patterns and pressure drops, Adv. Space Res., 16, pp. (7)137-(7)142.

Gnielinski, V. (1976). New Equations for Heat and Mass Transfer in Turbulent Pipe and Channel Flow, *Int. Chem. Eng.*, (16): 359 - 368.
Kim, T.H., Kommer, E., Dessiatoun, S., Kim, J. (2012). Measurement of two-phase flow and heat transfer parameters using infrared thermometry, *Int. J. Multiphase Flow,* 40 (2012) 56–67.
Lebaigue, O., Bouzou, N., Colin, C. (1998). Results from the Cyrène experiment: convective boiling and condensation of ammonia in microgravity, *28th Int. Conf. on Environmental Systems,* Danvers, Massachusetts.
Lockhart, R. W., Martinelli, R. C., (1949). Proposed Correlation of Data for Isothermal Two-Phase, Two-Component Flow in Pipes, Chemical Engineering Progress Symposium Series, **45** (1), pp. 39-48.
Lui, R.K., Kawaji, M., and Ogushi, T. (1994). An Experimental Investigation of Subcooled Flow Boiling Heat Transfer Under Microgravity Conditions, *10th International Heat Transfer Conference –Brighton*, Vol. 7, pp. 497-502.
Ma, Y., Chung, J.N. (2001). A Study of Bubble Dynamics in Reduced Gravity Forced-Convection Boiling, *Int. J. Heat Mass Transfer*, **44**, 399-415.
Nebuloni, S. And Thome, J.R. (2010). Numerical modeling of laminar annular film condensation for different channel shapes, *Int. J. Heat and Mass Transfer*, 53, 2615-2627.
Ohta, H. (1997). Experiments on Microgravity Boiling Heat Transfer by Using Transparent Heaters, *Nuclear Engineering and Design*, Vol. 175, pp. 167-180, 1997.
Ohta, H., Fujiyama, H., Inoue, K., Yamada, Y., Ishikura, and S., Yoshida, S. (1995). Microgravity Flow Boiling in a Transparent Tube, *Proc. 4th ASME-JSME Thermal Engineering Joint Conf.*, Lahina, Hawaii, USA, pp. 547–554.
Ohta, H. (2003). Microgravity heat transfer in flow boiling, *Advances in heat transfer*, Vol 37, 1-76.
Reinarts, T. R. (1993). *Adiabatic two phase flow regime data and modeling for zero and reduced (horizontal flow) acceleration fields*, PhD dissertation, Univ. of Texas A&M, 1993.
Rohsenow, W.M., Hartnett, J.P., Cho, Y.I. (1998). Forced convection, internal flow in ducts », *Handbook of Heat Transfer, Third Edition*, 5.2.
Saito, M., Yamaoka, N., Miyazaki, K., Kinoshita, M., and Abe, Y. (1994). Boiling Two-Phase Flow Under Microgravity, *Nuclear Engineering and Design*, Vol. 146, pp. 451-461.
Zhao, L., Rezkallah, K.S. (1993). Gas liquid flow patterns at microgravity conditions, *Int. J. Multiphase Flow,* 19, 751-763.
Zhao, L., Rezkallah, K.S. (1995). Pressure drop in Gas-Liquid flow at microgravity conditions Gas liquid flow patterns at microgravity conditions, *Int. J. Multiphase Flow*, 21, 837-849.
Zhao, L., Hu,W.R. (2000). Slug to annular flow transition of microgravity two-phase flow, *International Journal of Multiphase Flow* 26 , 1295-1304.